Geological, geophysical and geotechnical investigations into the internal structure and kinematics of an unstable, complex sliding mass in crystalline rock

H. Willenberg, K.F. Evans, E. Eberhardt & S. Loew
Engineering Geology, Swiss Federal Institute of Technology (ETH Zurich), Switzerland

T. Spillmann & H.R. Maurer
Applied and Environmental Geophysics, Swiss Federal Institute of Technology (ETH Zurich), Switzerland

ABSTRACT: Slope instabilities in massive crystalline rock are controlled by the internal structure of the rock mass which can be very complex. To understand the processes controlling the instability, it is necessary to identify the active discontinuities which govern the internal deformation, and to describe the kinematics of the unstable rock mass. In this paper we present results of a detailed analysis of the active features within an unstable gneissic rock mass of several million cubic meters volume from the Swiss Alps. The 3-D distribution of discontinuities within the rock mass was assessed using surface mapping and optical televiewer logs run in three boreholes drilled to depths of between 50 and 120 m. The subset of active fractures was identified from various types of surface displacement measurements and from surveys of inclinometer/extensometer casing installed in the boreholes. The active discontinuities were found to correspond to the major fractures which belong to an extensive network. Radar reflection profiles run in the boreholes showed that these active fractures extended significant distances from the borehole, in one case at least 49 m. Active fractures were found to be better reflectors of radar signals than inactive ones. The integration of all results was used to build a kinematic model describing the ongoing internal deformation of the rock mass.

1 INTRODUCTION

1.1 Investigation of the internal structure of unstable rock masses

Rock slope instabilities sometimes culminate in catastrophic failure involving high velocities or volumes which can cause great damage (Cruden & Varnes 1996). The specific mechanisms that control the development of instability towards catastrophic failure depend upon the internal structure of the rock mass. In massive crystalline rock slopes, the rock mass is usually dissected into multiple blocks by foliation-fractures, joints, fracture zones and faults, resulting in complex instability-related block movements. The estimation of the depth of the instability may be complicated in these cases since the basal boundary (sliding plane) might step through several fracture sets and involve fracturing of intact rock bridges (Einstein et al. 1983).

In 2002, an in-situ laboratory was established on a slowly moving crystalline rock mass high above the village of Randa in Switzerland as part of a multidisciplinary research project directed towards understanding the mechanisms underpinning slope instability in massive crystalline rock. Diverse geophysical, geological and geotechnical data describing the rock mass structure and kinematics have been collected since 2001. In this paper we focus on the analysis of the internal geological structure of the sliding rock mass and the geometrical properties of active fractures. This investigation is based on data from three steeply inclined boreholes (3D displacement and borehole georadar reflection measurements) in combination with data from surface fracture mapping and monitoring. The integration of these data yielded a detailed 3D-model of the structure of the unstable rock mass and the distribution of movements within this body..

1.2 Terminology for discontinuity mapping

The term *fracture* is used for structures that have accommodated only minor tectonic displacement, whereas *faults* are single shear fractures which form *fault zones* when several of them are interconnected. As the amount of differential displacement is difficult to quantify in polycyclic gneisses, faults are characterised by the presence of shear indicators like slickensides, Riedel fractures, or mylonitic, cataclastic or gouge-type fabrics. *Fracture zones* are characterised by intense fracturing occurring over dm-wide zones, where only minor differential displacement has been accommodated.

2 THE RANDA PROJECT SITE

The investigations were performed on a slowly moving rockslide on the western side of the North-South trending Matter Valley, near the village of Randa (Canton Valais) in the Swiss Alps (Figure 1). The moving rock mass lies at the top of the scarp formed by two major rockslides of 30 Mio m^3 that occurred in 1991 (documented by Schindler et al. 1993). The topography of the valley sides is steep, rising from the valley bottom at 1400 m a.sl. to high alpine summits above 4000 m a.sl., the unstable slope lying between ~1800 and 2400 m a.sl. The western slope of the valley consists of gneisses of the Penninic Siviez-Mischabel nappe of the Alpine Belt that dip into the slope at 25 degrees, which is, in principle, favourable for stability.

Figure 2 shows a map of the study area and the scarp of the 1991 rockslide. The shaded area denotes the extent of the unstable rock mass as derived from laser geodetic surveys (Ornstein et al. 2001). These measurements indicate annual surface displacements in the range of 1.5 – 2 cm The locations of three boreholes, SB120, SB50S and SB50N, drilled into the unstable rock mass to depths of 120, 50 and 50 m respectively are also shown. Multiple geophysical borehole logs and seismic and radar surveys were conducted before inclinometer/extensometer casings, equipped with piezometers and seismometers, were cemented in-place. The inclinometer/ extensometer casings are surveyed twice a year to provide a profile of displacements occurring along the boreholes. In this paper we relate the displacement profiles to the internal geological structure of the rock mass which is derived using surface mapping and borehole televiewer and radar data.
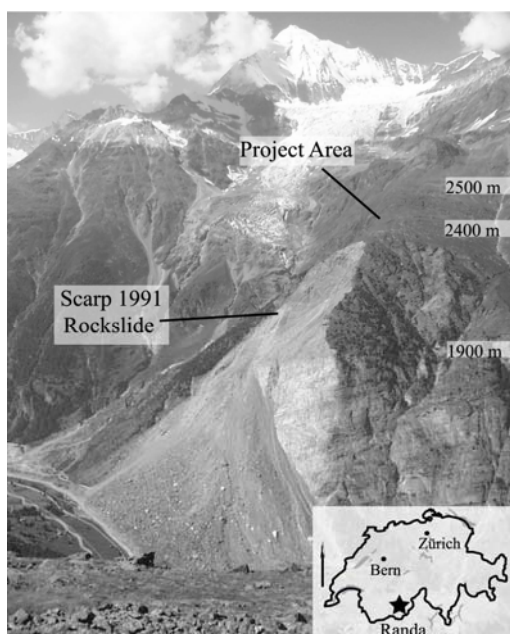
Figure 1. Photo of the Randa project site: Project area and scarp of the 1991 rockslide.
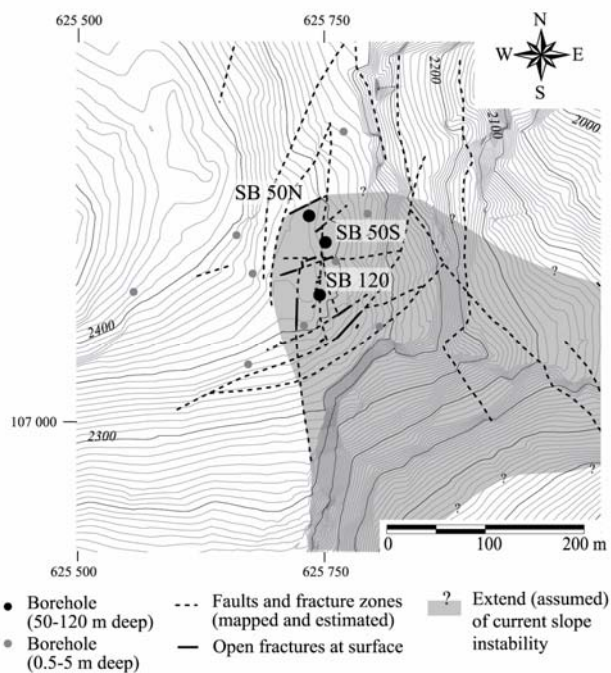
Figure 2. Project area and location of the deep and shallow boreholes. The assumed extent of the current instability is indicated in grey. Dashed lines show the position of mapped faults and fracture zones; active segments are highlighted with solid lines.

3 MAPPING AND CHARACTERISATION OF ACTIVE FRACTURES

3.1 Discontinuity mapping and displacement surveys

Based on surface mapping, two scales of discontinuity networks were recognised: a small-scale network consisting of fractures with lengths of up to 5 m, and a large-scale network of faults and fracture zones. The small-scale network consists of four steep and two inclined fractures sets (Figure 3a). Trace lengths were found to follow lognormal distributions with mean trace lengths between 1.0 and 1.3 m for the steep fracture sets and 3.3 m for the foliation fractures. No evidence of active displacement was found for the small-scale fractures. Faults and fracture zones have trace lengths longer than 10 m. A fault map for the study area is shown in Figure 2. The figure reveals two dominant orientations of inclined and steep faults that strike N-S and NE-SW. Most faults and fracture zones in the vicinity of the boreholes were equipped with crackmeters and benchmark arrays, and some were found to support active relative displacements of up to 0.6 cm/yr (Figure 2). Thus the surface observations indicate that displacements within the rock mass are mainly controlled by the large-scale fault and fracture-zone network.

a)   Small-scale fractures at surface

b)   Minor fractures in the boreholes
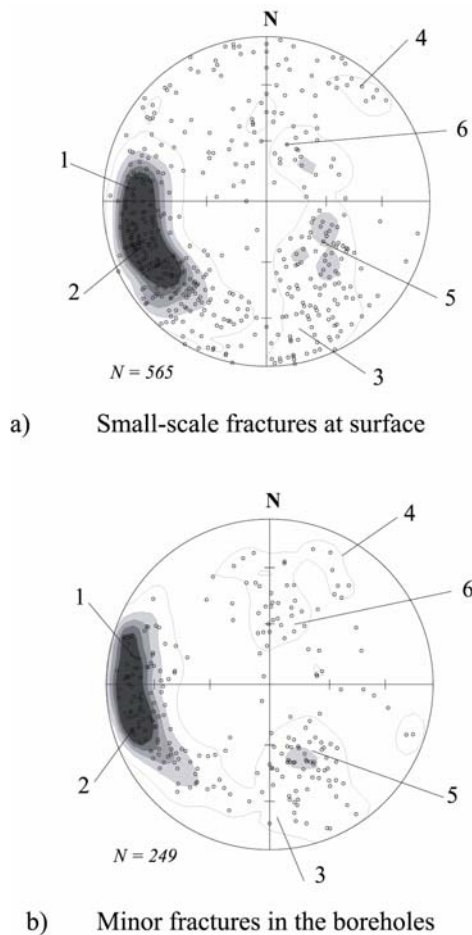
Figure 3. Stereonets of fractures in the study area (lower hemisphere plot, equal area projection; isolines follow 5,10,15,20% densities; foliation fractures are not plotted). a) Small-scale fracture network mapped at surface. b) Minor fractures mapped within the boreholes SB120, SB50S and SB50N. At surface and at depth six fractures sets with comparable orientations were identified.

The surface mapping was extended into 3-D using oriented optical televiewer images from the 3 boreholes. The images allowed the dip, dip-direction and rank (i.e. minor or major fractures) to be determined, the latter from the thickness of the fracture trace on the image. Fractures with traces below 1-2 mm thickness were categorised as minor fractures. The orientation characteristics of the borehole fracture sets (Figure 3b) were in accord with surface observations. The traces of major fractures encountered in SB120 are shown in the wrap-around image of Figure 4c. These fractures have widths greater than 2 mm and tend to contain intensely foliated material.

The total number of fractures per inclinometer interval (0.61 m) is shown alongside in Figure 4b together with the displacement profile derived from inclinometer/extensometer surveys. The displacement profile represents the magnitude of the 3D displacement vector per unit measurement interval (0.61 m). The peaks denote active zones between blocks where relative displacement has occurred (for

explanation of the analysis procedure see Willenberg et al. 2003). Most peaks are contained within one measurement interval, indicating that the deformation is highly localised. In all cases, the peaks can be correlated with distinct major fractures. In contrast, regions of high fracture density (i.e. more than 3 fractures per 0.61 m) generally do not exhibit distributed displacement. Thus, internal deformation of the rock mass is accommodated solely by dislocation of the active major fractures. In the case of SB120, 12 out of 20 major fractures were found to be active (the active fractures are labelled in regular font in Figure 4c).

Regarding the internal rock mass structure and kinematics, two important questions have to be addressed: i) how far do the active features extend into the rock mass, and ii) whether they are planar. Borehole radar reflection surveys were used to address these issues.

3.1.1   Single-hole georadar reflections

The principle of the single-hole radar method is shown in Figure 5a. By moving the transmitter and receiver antennae at constant offset along the borehole, an image of reflecting objects is acquired. In case of planar fractures intersecting the borehole, the reflected signals form hyperbolic patterns (Figure 5b). The travel time t of such reflections is governed by the equation

$$t = \frac{2}{v}\sqrt{z^2 \sin^2 \Theta + c^2 \cos^2 \Theta} \qquad (1)$$

in which v = velocity, Θ = angle between the borehole and the fracture plane, $2c$ = antenna offset and z = antenna midpoint distance from intersection point (Olsson et al. 1992).

Georadar data acquired in borehole SB120 revealed 6 hyperbolic features that could be associated with planar fractures (dashed lines in Figure 4d). No signal energy was recorded close to the hyperbolas apexes. Here, transmitter and receiver are on opposite sides of the fracture and thus no reflection can occur.

Using a constant velocity v=0.12 m/ns that was obtained from a cross-hole experiment between boreholes SB50N and SB50S, we predicted reflection travel times corresponding to the major fractures delineated in the televiewer log (Figure 4c). Six out of the twenty predictions could be associated with the hyperbolic reflections patterns observed in the georadar section (grey shaded areas denoted A to F in Figure 4d). A reasonably good fit is observed with the exception of prediction D.

The small deviations found for predictions A to F are likely caused by curvatures of the reflectors, but the assumption of planar fractures seems to be generally well justified.
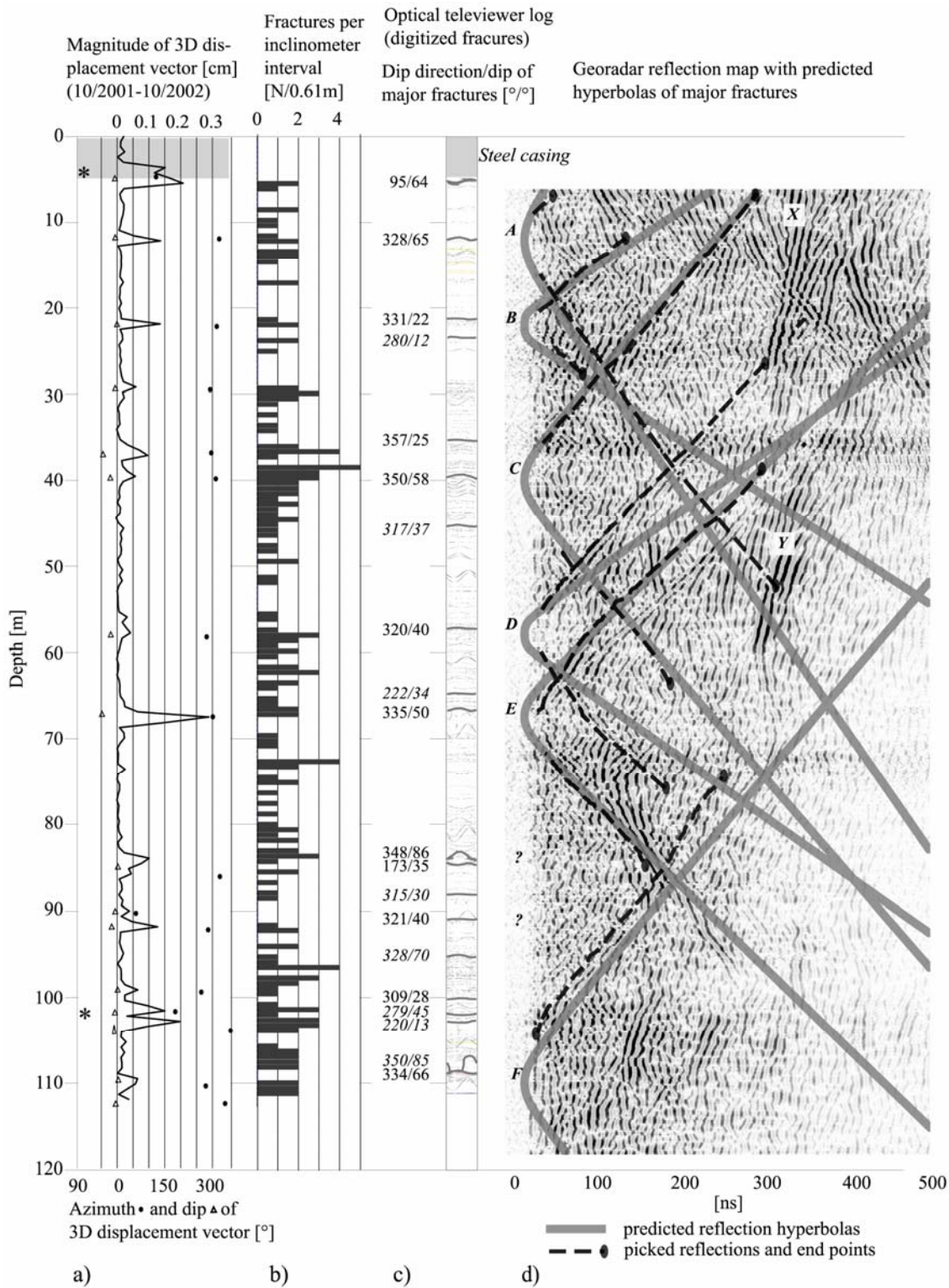
Figure 4. Fracture mapping in SB120. a) Incremental displacement magnitude along the hole and azimuth, θ and dip, φ, of the relative displacement vectors. The stars at 5 and 103 m denote zones where casing deformation is related to ungrouted sections. b) Number of fractures per inclinometer interval (0.61m) derived from the optical televiewer image. c) Digitised fracture traces on the optical televiewer image. Major fractures are highlighted and dip-direction and dip supplied. d) Georadar reflection image with predicted (solid) and picked (dashed) reflections. Six predictions that could be associated with georadar reflections are shown.
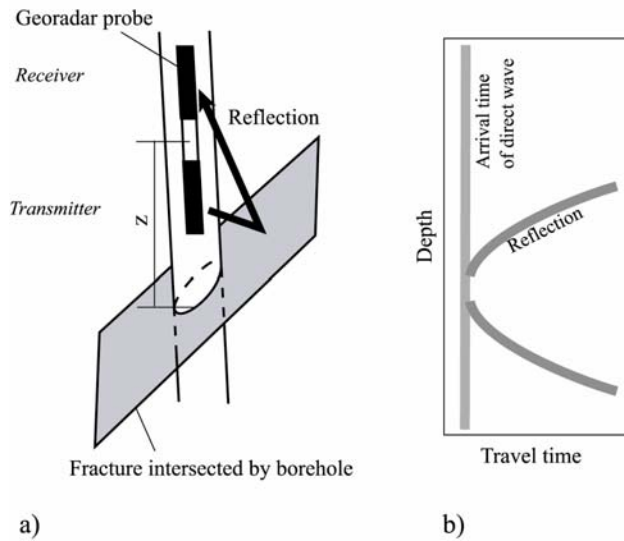
Figure 5. Principle of the single-hole georadar reflection method. a) Fracture plane reflects georadar signal. b) The characteristic reflection pattern generated by a planar reflector.

The discrepancy observed for prediction D could be related to a step-like fracture offset occurring exactly at the borehole intersection. An important feature of the georadar data is their capability to trace the fractures away from the boreholes. In particular, the extensions of the hyperbolic reflection patterns allow minimum fracture lengths to be determined.

Applying basic migration principles (Yilmaz 2001) to pattern end points, minimum extensions be-

tween 7.8 and 49 m were determined. The effective extensions may be longer, but strong reflections, possibly caused by more distant fractures not intersecting the borehole (denoted X and Y in Figure 4d), obscure the hyperbolic patterns.

The minimum length estimates indicate that all fractures observed in the georadar data must be significant. This was confirmed by inclinometer and extensometer data recorded in the same borehole. Figure 4 clearly shows that six active fractures could be associated with georadar reflections, whereas no correlation with inactive fractures was found. These results from the Randa test site suggest that only active fractures manifest themselves in georadar reflections. It would be a topic of future research, if this finding can be generalized.

3.2 Internal structure of the investigated slope

Based on the borehole displacements and radar results, a block kinematic model for the unstable rock mass was constructed to attempt to discriminate between different types of rock mass kinematic behaviour. For example whether displacement is localised and accommodated on a few, extensive through-going planar features or whether it is distributed throughout the rock mass, perhaps stepping through the various steep and inclined fracture sets of a small-scale fracture network. The block model is shown in Figure 6. The results imply that at Randa,
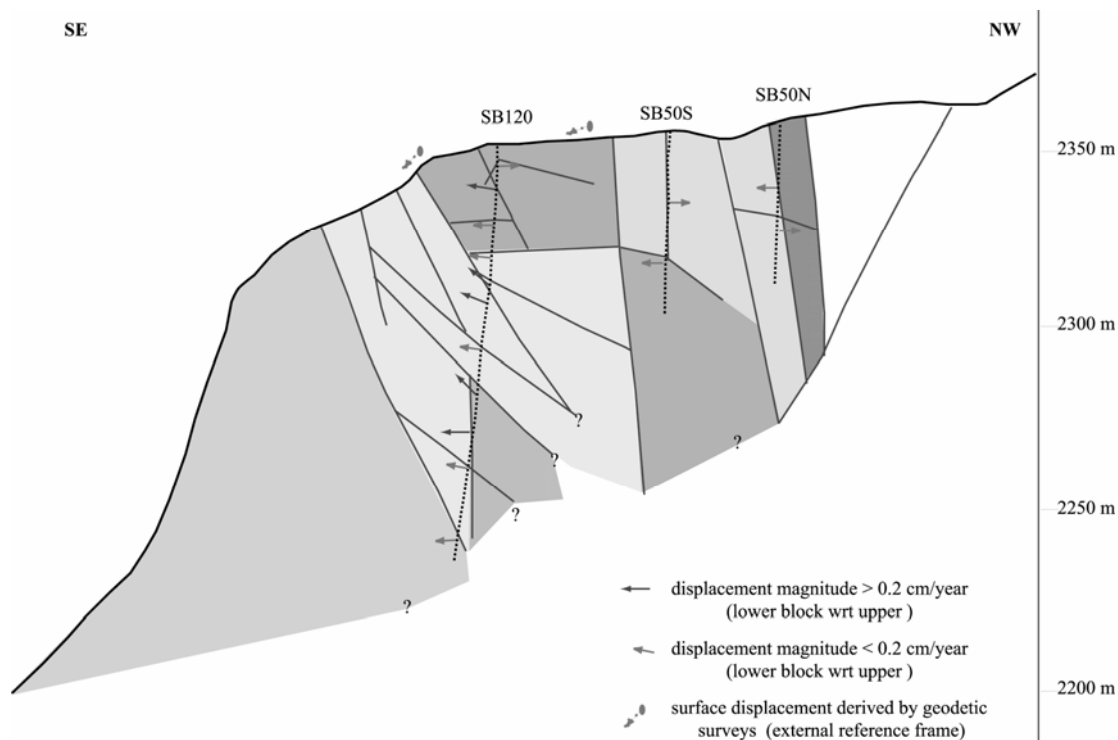
Figure 6. Preliminary block model showing the internal structure of the unstable rock mass. Solid lines define extrapolated faults and fracture zones, whereas the arrows indicate displacement directions (lower block wrt the upper) for a one-year inter-survey time (axial strain is measured only in SB120). Surface displacements are plotted wrt to an external reference frame.

active displacements within the rock mass to the depth of the boreholes are accommodated by dislocation of the faults and fracture zones of the large-scale network. No evidence for the presence of large active fractures parallel to the absolute surface displacement vector was found, a result that contradicts the assumptions of published models (e.g. Sartori et al. 2003).

The relative displacement vectors across block boundaries intersected by the three boreholes are shown in Figure 6 (vector drawn on lower block with respect to upper). The general trend is for lower blocks to be displaced towards the SE, the same direction as the absolute surface displacement derived from long-baseline geodetic surveys. Thus, the magnitude of the absolute displacement vectors increases with depth.

4 CONCLUSIONS

The internal structure of a slowly moving rockslide in massive crystalline rock has been constrained successfully by the integration of discontinuity mapping at surface and in boreholes, of borehole displacement surveys and of single-hole georadar reflections. Analysing single-hole georadar reflections with a travel time prediction scheme provided values to constrain active fracture persistence into the rock mass behind the borehole wall. Based on this information, a model of the internal structure could be developed. This model is the basis for the interpretation of the rockslide kinematics and provides block geometries and displacements for numerical modelling of rockslide processes.

REFERENCES

Cruden, D. & Varnes, D. J. 1996. Landslide types and processes. in A. K. Turner & R. L. Schuster (eds). Landslides: investigation and mitigation: 36-75. Washington - National Academy Press.

Einstein, H. H., Veneziano, D., Baecher, G. B. & O'Reilly, K. J. 1983. The effect of discontinuity persistence on rock slope stability. *International Journal of Rock Mechanics and Mining Sciences 20*(1): 227-236.

Olsson, O., Falk, L., Forslund, O., Lundmark, L. & Sandberg, E. 1992. Borehole radar applied to the characterization of hydraulically conductive fracture zones. *Geophysical Prospecting 40*: 109-142.

Ornstein, P., Jaboyedoff, M. & Rouiller, J. D. 2001. Surveillance géodésique du site de Randa (VS): gestion des mesures 1-D et 3-D. In *Herbsttagung der Schweizerischen Gesellschaft für Boden- und Felsmechanik*.

Sartori, M., Baillifard, F., Jaboyedoff, M. & Rouiller, J. D. 2003. Kinematics of the 1991 Randa rockslides (Valais, Switzerland). *Natural Hazards and Earth System Sciences 3*: 423-433.

Schindler, C., Cuénod, Y., Eisenlohr, T. & Joris, C. L. 1993. Die Ereignisse vom 18. April und 9. Mai 1991 bei Randa (VS) - ein atypischer Bergsturz in Raten. *Eclogae Geologicae Helvetiae 86*(3): 643-665.

Willenberg, H., Evans, K. F., Eberhardt, E. & Loew, S. 2003. Monitoring complex rock slope instabilities - correction and analysis of inclinometer/extensometer surveys and integration with surface displacement data. In F. Myrvoll (ed) *Sixth International Symposium on Field Measurements in Geomechanics*, *Oslo*: Balkema.

Yilmaz, Ö. 2001. Seismic data analysis - processing, inversion and interpretation of seismic data. Tulsa - Society of Exploration Geophysicists.